Journal of Electrostatics 70 (2012) 166–173

Contents lists available at SciVerse ScienceDirect

Journal of Electrostatics

journal homepage: www.elsevier.com/locate/elstat

Electrostatic force between rings and discs of charge inside a grounded metallic pipe using the Green's function technique

Daniel T. Lopes [a], Cláudio C. Motta [b,*]

[a] Instituto de Pesquisas Energéticas e Nucleares (IPEN), São Paulo, SP, Brazil
[b] Universidade de São Paulo (USP), Av. Prof. Lineu Prestes 2468, 05508-000 Sao Paulo, SP, Brazil

ARTICLE INFO

Article history:
Received 14 May 2011
Received in revised form
9 October 2011
Accepted 11 December 2011
Available online 24 December 2011

Keywords:
Green's function technique
Ring and disc charge potential and field distributions
Cosine Fourier transforms

ABSTRACT

We derive analytic formulae for the electrostatic force between ring and disc charge distributions inside a grounded metallic pipe using the Green's function technique. These distribution models are useful in the modeling of electron beams commonly employed in microwave tubes. We analyze the electric force between two discs, between two rings, and between a disc and a ring and we compare the results for the electric potential, field, and force to numerical ones obtained from a 3D electrostatic solver. Present expressions were developed to avoid an oscillatory noise when the field diverges by axial proximity between source and observer.

© 2011 Elsevier B.V. All rights reserved.

1. Introduction

Among microwave-vacuum-electronic devices (MVEDs), traveling-wave tubes (TWTs) and klystron amplifiers present outstanding performances in the amplification of radio frequency (RF) signals at high-power levels in microwave and millimeter-wave frequencies. Klystron amplifiers also find relevant applications in charged particle accelerator technologies. Klystrons and TWTs amplify RF signals by providing the necessary conditions for the kinetic energy of an accelerated electron beam (e-beam) be converted in electromagnetic field strength. Therefore, accurate beam-wave interaction modeling tools are essential for the improvement of the efficiency of MVEDs.

In commercial 3D modeling tools for MVEDs, the particle-in-cell (PIC) [1–3] technique has been successfully used to model the beam-wave interaction phenomenon. In the PIC approach, the electromagnetic fields are calculated in a background grid, while fields on the particle are evaluated interpolating the field values of the surrounding cell. The accuracy of PIC simulations is directly proportional to the number of particles and inversely proportional to the grid cell size. These features require high computational power, thus, PIC codes are more likely used in the fine-tuning steps of the MVED design. On the other hand, in the earlier design steps, analytical and semi-analytical codes are preferred due to the much smaller computation time necessary to obtain preliminary results and due to the more physical insight [4,5]. By semi-analytical codes we mean codes that numerically integrate particle dynamics equations considering the electric force contribution of every particle in the system. This approach is sometimes called particle-to-particle simulation and uses the Green's function technique to obtain the electric force among particles for a given geometry domain and an assumed particle charge distribution, such as planes, points, discs, rings, etc.

The usual way to modeling the electron transport, in beam-wave problems, is to split the electric forces in two contributions. The first force, object of this work and always present, is due to the electrostatics forces between the particles only, and therefore the Green's function technique is a very useful tool. After solving the electrostatic problem and checking the electron transport beam dynamics, the RF contribution, time dependent, responsible to the beam velocity modulation, is turned on to complete the description.

Though electric potential and field expressions are not difficult to find in the literature, as those between tips and metallic flat surfaces based on a generalized image-charge method [6,7], the authors have no knowledge about force expressions among discs and rings of charge inside a grounded metallic pipe in the specialized literature [8,9]. This lack motivated us to derive such

* Corresponding author. Tel.: +55 11 3817 7256; fax: +55 11 3817 7110.
E-mail addresses: danieltl@usp.br (D.T. Lopes), ccmotta@usp.br (C.C. Motta).

0304-3886/$ – see front matter © 2011 Elsevier B.V. All rights reserved.
doi:10.1016/j.elstat.2011.12.006

expressions. Furthermore, the electric field expressions for ring particles presented in [5] use a Green's function expansion that leads to oscillatory noise in the electric field values when the source and the observer axial coordinates tend to each other [9]. In the present work, we use another kind of Green's function expansion in order to transfer the oscillatory noise to the radial coordinate. Depending on the problem faced, one or other approach is more suitable. For instance, particle overtake is a common phenomenon in beam-wave interaction at large signal regime. If the overtakes are assumed to predominantly occur in axial coordinate, the oscillatory noise that occurs when source and observer axial coordinates tend to each other should be avoided. On the other hand, if radial overtake is a major issue, the otherwise case takes place. Therefore, we present here an alternative approach for the same problem.

This paper is organized as follows: In Section 2, we present the expressions for the Green's function inside a grounded metallic pipe; for the electric potential and the electric field generated inside the pipe; and for the electric force between a pair of particles (ring and disc). In Section 3, we present plots for those expressions, comparing the analytical results to numerical ones obtained from a 3D electrostatic solver. We also compare the present ring electric potential and ring electric field analytic results to the referred expressions in the literature [7]. Finally, we present a conclusion in Section 4. In the appendix, we briefly present the main steps in the derivation of the Green's functions used.

2. The electric potential, field and force expressions

The main purpose of this work consists in evaluating the interaction forces among the charged particles that compose an e-beam model. Let's consider the pencil beam model, which the axial cross section is illustrated in Fig. 1(a). The e-beam is formed by a core of charged discs on the axis inside a grounded metallic pipe with radius a. The discs are surrounded by concentric infinitesimally thin charged rings with charge proportional to their initial perimeter. This kind of e-beam model is often used in 2D and 2.5D space charge simulations. The disks are assumed to move only on axis. Evidently, due to the azimuthal symmetry of the problem, the radial components of those forces are null. Therefore, in the 2D model, the observer ring is represented by the ring element and the radial force is actually evaluated on the ring element. Fig. 1(b) shows a 2D view of the beam model and the force scheme considered. The force between two discs is denoted by $\mathbf{F}_{dd} = F_{dd}\hat{\mathbf{z}}$, containing only the axial component. The force between two rings is $\mathbf{F}_{rr} = F_{\rho}^{rr}\hat{\boldsymbol{\rho}} + F_{z}^{rr}\hat{\mathbf{z}}$, which contains both the axial and the radial components. The force between a disc and a ring is $\mathbf{F}_{dr} = -\mathbf{F}_{rd} = F_{\rho}^{dr}\hat{\boldsymbol{\rho}} + F_{z}^{dr}\hat{\mathbf{z}}$, where $\mathbf{F}_{rd}$ is the reciprocal force, $\hat{\boldsymbol{\rho}} = \hat{\boldsymbol{\rho}}(\varphi)$ and $\hat{\mathbf{z}}$ denote the radial and the axial unit vectors in the cylindrical coordinate system, respectively. The radial force components are evaluated on the observer ring element.

Assuming that all source particles are axially concentric inside a grounded metallic pipe, the force that a source particle exert on another one in the observer position is given by

$$\mathbf{F} = \int_V \varrho(\mathbf{r})\mathbf{E}(\mathbf{r})d^3\mathbf{r}, \tag{1}$$

where $\varrho(\mathbf{r})$ is the charge distribution of the observer particle and $\mathbf{E}(\mathbf{r})$ is the electric field measured in the observer position $\mathbf{r}$, generated by the source particle, which lies in the source position $\mathbf{r}'$. For infinitesimally thin ring particles, the source charge distribution is given by

$$\varrho_r(\mathbf{r}) = \varrho_r(\rho, z) = \frac{q_r}{2\pi\rho'}\delta(\rho-\rho')\delta(z-z'). \tag{2}$$

On the other hand, the disc charge distribution is written as

$$\varrho_d(\mathbf{r}) = \varrho_d(\rho, z) = \begin{cases} \dfrac{q_d}{\pi\rho'^2}\delta(z-z') & 0 \le \rho \le \rho' \\ 0 & \rho' < \rho \le a \end{cases}, \tag{3}$$

where ρ' and z' are the source particle radial and axial coordinates, respectively, and q_r and q_d are the electric charge contained in the ring and in the disc, respectively. In Eqs. (2) and (3), $\delta(\mathbf{r}-\mathbf{r}')$ is the Dirac's delta function. It has to be mentioned that the observer ring charge distribution is different from the source. It is obtained by multiplying Eq. (2) by $2\pi\delta(\varphi-\varphi')$. It must be understood that (ρ', φ', z') are, in this case, the observer coordinates.

The electric field is obtained in the usual way by differentiating the electric potential with respect to each coordinate, i.e., $E_z(\rho,z) = -\partial\Phi(\mathbf{r})/\partial z$ and $E_\rho(\rho,z) = -\partial\Phi(\mathbf{r})/\partial\rho$. Since all particles are inside a grounded metallic pipe, the electric potential, solution of Poisson equation, is obtained by means of the Green's theorem with vanished surface integral, i.e.,

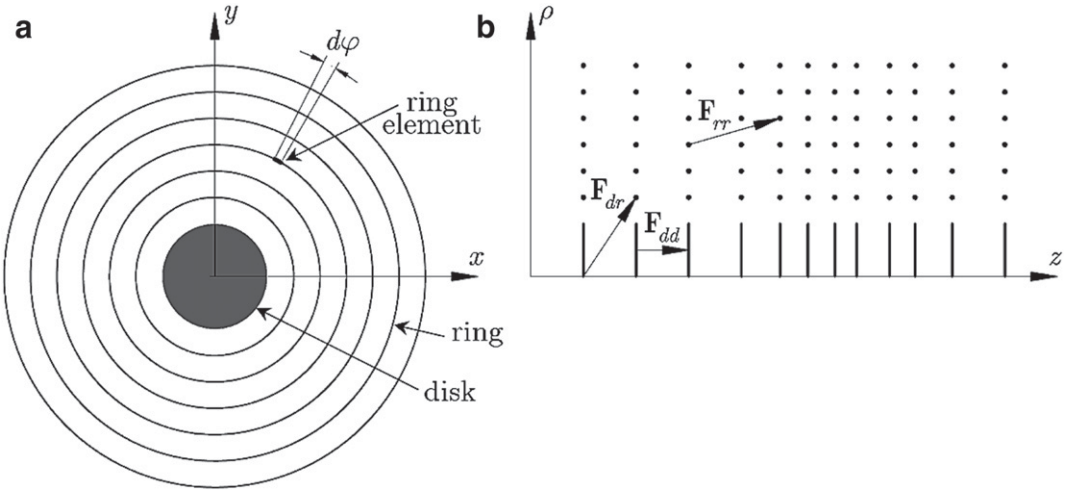

Fig. 1. (a) Axial cross section of the e-beam model formed by a stiff charged disk core and charged rings around it. (b) A 2D view of the e-beam model showing the three forces considered, namely, $\mathbf{F}_{dd}$ is the force between two disks, $\mathbf{F}_{rr}$ is the force between a source ring and an observer element ring, and $\mathbf{F}_{dr}$ is the force between a source disk and an observer element ring.

$$\Phi(\mathbf{r}) = \frac{1}{\varepsilon_0}\int_{V'} \rho(\mathbf{r}')G(\mathbf{r},\mathbf{r}')d^3\mathbf{r}', \tag{4}$$

where $G(\mathbf{r},\mathbf{r}')$ is the Green's function for the Laplace's equation inside a grounded metallic pipe, which must satisfy

$$\nabla^2 G(\mathbf{r},\mathbf{r}') = -\delta(\mathbf{r}-\mathbf{r}') \tag{5}$$

and the homogeneous Dirichlet boundary condition

$$\begin{cases} G(\rho = a) = 0 \\ G(z \to \pm\infty) = 0 \end{cases}. \tag{6}$$

2.1. Green's functions

The derivation of the present Green's functions is briefly described in the appendix. Here, we discuss about the type of expansion used in the two equivalent Green's function representation. For the disc problem, we used the following Green's function

$$\Phi_r(\rho,z) = \frac{q_r}{2\pi^2\varepsilon_0}\begin{cases} \displaystyle\int_0^\infty \left[K_0(kb_r) - \frac{K_0(ka)}{I_0(ka)}I_0(kb_r)\right] I_0(k\rho)\cos[k(z-z_r)]dk, & 0 \le \rho \le b_r \\ \displaystyle\int_0^\infty \left[K_0(k\rho) - \frac{K_0(ka)}{I_0(ka)}I_0(k\rho)\right] I_0(kb_r)\cos[k(z-z_r)]dk, & b_r \le \rho \le a, \end{cases} \tag{10}$$

$$G_1(\mathbf{r},\mathbf{r}') = \frac{1}{2\pi a}\sum_{m=-\infty}^{\infty}\sum_{n=1}^{\infty}\frac{J_m(x_{m,n}\rho/a)J_m(x_{m,n}\rho'/a)}{x_{m,n}J_{m+1}^2(x_{m,n})} \times e^{jm(\varphi-\varphi')}e^{-\frac{x_{m,n}}{a}|z-z'|}, \tag{7}$$

while, for the ring problem, we used

$$G_2(\mathbf{r},\mathbf{r}') = \frac{1}{2\pi^2}\sum_{m=-\infty}^{\infty} e^{jm(\varphi-\varphi')}\int_0^\infty \left[K_m(k\rho_>) - \frac{K_m(ka)}{I_m(ka)}I_m(k\rho_>)\right] \times I_m(k\rho_<)\cos[k(z-z')]dk, \tag{8}$$

where $\rho_>(\rho_<)$ is the larger (smaller) of ρ and ρ' [8,9]. $J_m()$ is the ordinary Bessel's function of order m, while $x_{m,n}$ is its n-th zero. $I_m()$ and $K_m()$ are the modified Bessel's functions of the first and second kind, respectively, and order m.

One may verify that Eqs. (7) and (8) are numerically identical. The use of ordinary Bessel's functions in Eq. (7) and modified Bessel's functions in Eq. (8) is due to the kind of expansion used in the Green's function construction. In Eq. (7), we expanded $G_1(\mathbf{r},\mathbf{r}')$ in terms of radial and azimuthal eigenfunctions, solutions of the Laplace's problem inside the metallic pipe. In Eq. (8), we expanded $G_2(\mathbf{r},\mathbf{r}')$ in terms of azimuthal and axial eigenfunctions, solutions of the Laplace's problem for the same case. When we analyze the discontinuity of the first derivative of the Green's function, i.e., the electric field, we find that it becomes noisy when z tends to z', while the field derived from Eq. (8) becomes noisy when ρ tends to ρ'. Depending on the problem, one or other approach may be more suitable.

2.2. Electric potentials

The electric potential generated inside the metallic pipe by a disc of radius b_d and electric charge q_d on the axial position z_d is obtained using Eqs. (7) and (3) in Eq. (4), resulting in

$$\Phi_d(\rho,z) = \frac{q_d}{\pi\varepsilon_0 b_d}\sum_{n=1}^{\infty}\frac{J_1(x_{0,n}b_d/a)}{x_{0,n}^2J_1^2(x_{0,n})}J_0\left(\frac{x_{0,n}}{a}\rho\right)e^{-\frac{x_{0,n}}{a}|z-z_d|}. \tag{9}$$

On the other hand, the electric potential generated inside the metallic pipe by a ring of radius b_r and electric charge q_r on the axial position z_r is obtained using Eqs. (8) and (2) in Eq. (4), resulting in which is numerically identical to Eq. (9) in [5], however with different behavior with respect to convergence as the observer gets closer to the source position.

2.3. Electric fields

The electric field generated by a disc having radius b_d with a charge q_d at z_d inside the metallic pipe writes $\mathbf{E}_d(\mathbf{r}) = E_\rho^d(\rho,z)\hat{\boldsymbol{\rho}} + E_z^d(\rho,z)\hat{\mathbf{z}}$, where

$$E_\rho^d(\rho,z) = \frac{q_d}{\pi\varepsilon_0 ab_d}\sum_{n=1}^{\infty}\frac{J_1(x_{0,n}b_d/a)}{x_{0,n}J_1^2(x_{0,n})}J_1\left(\frac{x_{0,n}}{a}\rho\right)e^{-\frac{x_{0,n}}{a}|z-z_d|}, \tag{11}$$

$$E_z^d(\rho,z) = \frac{z-z_d}{|z-z_d|}\frac{q_d}{\pi\varepsilon_0 ab_d}\sum_{n=1}^{\infty}\frac{J_1(x_{0,n}b_d/a)}{x_{0,n}J_1^2(x_{0,n})}J_0\left(\frac{x_{0,n}}{a}\rho\right)e^{-\frac{x_{0,n}}{a}|z-z_d|}. \tag{12}$$

Additionally, the electric field generated by a ring having radius b_r with a charge q_r at z_r inside the metallic pipe is written as $\mathbf{E}_r(\mathbf{r}) = E_\rho^r(\rho,z)\hat{\boldsymbol{\rho}} + E_z^r(\rho,z)\hat{\mathbf{z}}$, where

We also present, in the results section, plots of the electric field for disc and rings together with a comparison with numerical

$$E_\rho^r(\rho,z) = \frac{q_r}{2\pi^2\varepsilon_0}\begin{cases} -\displaystyle\int_0^\infty \left[K_0(kb_r) - \frac{K_0(ka)}{I_0(ka)}I_0(kb_r)\right] I_1(k\rho)\cos[k(z-z_r)]kdk, & 0 \le \rho < b_r \\ \displaystyle\int_0^\infty \left[K_1(k\rho) + \frac{K_0(ka)}{I_0(ka)}I_1(k\rho)\right] I_0(kb_r)\cos[k(z-z_r)]kdk, & b_r < \rho \le a \end{cases} \tag{13}$$

$$E_z^r(\rho,z) = \frac{q_r}{2\pi^2\varepsilon_0}\begin{cases} \displaystyle\int_0^\infty \left[K_0(kb_r) - \frac{K_0(ka)}{I_0(ka)}I_0(kb_r)\right] I_0(k\rho)\sin[k(z-z_r)]kdk, & 0 \le \rho < b_r \\ \displaystyle\int_0^\infty \left[K_0(k\rho) - \frac{K_0(ka)}{I_0(ka)}I_0(k\rho)\right] I_0(kb_r)\sin[k(z-z_r)]kdk, & b_r < \rho \le a \end{cases}. \tag{14}$$

results from a finite element 3D electrostatic solver [3]. We show an additional comparison between Eqs. (13) and (14) and electric field equations Eq. (12) given in [5], in order to show the difference between the two approaches when the observer gets closer to the source ring.

2.4. Electric forces

Since the expressions for the electric fields produced by rings and discs have been derived, the electric force between a pair of these particles can be calculated using Eq. (1). Considering a source disc with electric charge $q_{d,s}$ and radius $b_{d,s}$ on the axial position $z_{d,s}$, the force applied on another disc with electric charge $q_{d,o}$ and radius $b_{d,o}$ on the observer axial position $z_{d,o}$ is given by $\mathbf{F}_{dd} = F_{dd}\hat{\mathbf{z}}$, where

$$F_{dd} = \frac{z_{d,o}-z_{d,s}}{|z_{d,o}-z_{d,s}|}\frac{2}{\pi\varepsilon_0}\frac{q_{d,s}q_{d,o}}{b_{d,s}b_{d,o}} \times \sum_{n=1}^{\infty}\frac{J_1(x_{0,n}b_{d,s}/a)J_1(x_{0,n}b_{d,o}/a)}{x_{0,n}^2J_1^2(x_{0,n})}e^{-\frac{x_{0,n}}{a}|z_{d,o}-z_{d,s}|}. \quad (15)$$

If both discs have the same electric charge and radius, Eq. (15) becomes more compact. Considering now a source ring with electric charge $q_{r,s}$ and radius $b_{r,s}$ on the axial position $z_{r,s}$, the applied force on a ring element with electric charge $q_{r,o}$, radius $b_{r,o}$, on the axial $z_{r,o}$, and azimuthal $\varphi_{r,o}$ observer positions, is given by $\mathbf{F}_{rr} = F_{\rho}^{rr}\hat{\boldsymbol{\rho}}(\varphi_{r,o}) + F_z^{rr}\hat{\mathbf{z}}$, where

$$F_{\rho}^{rr} = \frac{q_{r,s}q_{r,o}}{2\pi^2\varepsilon_0}\begin{cases} -\int_0^{\infty}\left[K_0(kb_{r,s}) - \frac{K_0(ka)}{I_0(ka)}I_0(kb_{r,s})\right]I_1(kb_{r,o})\cos[k(z_{r,o}-z_{r,s})]kdk, & b_{r,o}<b_{r,s} \\ \int_0^{\infty}\left[K_1(kb_{r,o}) + \frac{K_0(ka)}{I_0(ka)}I_1(kb_{r,o})\right]I_0(kb_{r,s})\cos[k(z_{r,o}-z_{r,s})]kdk, & b_{r,o}>b_{r,s} \end{cases}, \quad (16)$$

and

$$F_z^{rr} = \frac{q_{r,s}q_{r,o}}{2\pi^2\varepsilon_0}\begin{cases} \int_0^{\infty}\left[K_0(kb_{r,s}) - \frac{K_0(ka)}{I_0(ka)}I_0(kb_{r,s})\right]I_0(kb_{r,o})\sin[k(z_{r,o}-z_{r,s})]kdk, & b_{r,o}<b_{r,s} \\ \int_0^{\infty}\left[K_0(kb_{r,o}) - \frac{K_0(ka)}{I_0(ka)}I_0(kb_{r,o})\right]I_0(kb_{r,s})\sin[k(z_{r,o}-z_{r,s})]kdk, & b_{r,o}>b_{r,s} \end{cases}, \quad (17)$$

The force that a disc of radius b_d and electric charge q_d in the source axial position z_d apply on the ring element with radius $b_r > b_d$ and electric charge q_r in the axial $z_{r,o}$, and azimuthal $\varphi_{r,o}$ observer positions, is given by $\mathbf{F}_{dr} = F_{\rho}^{dr}\hat{\boldsymbol{\rho}}(\varphi_{r,o}) + F_z^{dr}\hat{\mathbf{z}}$, where

$$F_{\rho}^{dr} = \frac{q_dq_r}{\pi\varepsilon_0ab_d}\sum_{n=1}^{\infty}\frac{J_1(x_{0,n}b_d/a)J_1(x_{0,n}b_r/a)}{x_{0,n}J_1^2(x_{0,n})}e^{-\frac{x_{0,n}}{a}|z_r-z_d|}, \quad (18)$$

$$F_z^{dr} = \frac{z_r-z_d}{|z_r-z_d|}\frac{q_dq_r}{\pi\varepsilon_0ab_d}\sum_{n=1}^{\infty}\frac{J_1(x_{0,n}b_d/a)J_0(x_{0,n}b_r/a)}{x_{0,n}J_1^2(x_{0,n})}e^{-\frac{x_{0,n}}{a}|z_r-z_d|}. \quad (19)$$

Plots of the force between pairs of each particle and a comparison with numerical results from a 3D electrostatic solver are shown the results section.

3. Results

In this section, we show plots for the expressions presented above. Additionally, we compare the analytic results to numerical ones obtained from a finite element 3D electrostatic solver [3]. Furthermore, for the ring case, we show a comparison with referred expressions, which are Eqs. (9) and (12) in [5]. In the following plots, we defined the normalized electric potential as $\Phi\varepsilon_0 a/q$, the normalized electric field is $\mathbf{E}\varepsilon_0 a^2/q$, and the normalized electric force is $\mathbf{F}\varepsilon_0 a^2/q_sq_o$. We also normalized the axial position as $(z_o-z_s)/a$ and the radial position as ρ/a.

3.1. Disc particle results

In these plots, the source disc always has radius $b_d = a/2$ and lies on the axial position $z = 0$. Fig. 2 shows the normalized radial electric field as a function of the normalized radial position for two axial positions. In $z = 0$, we observe a noise in the analytic solution, which is a characteristic of the expansion used in Eq. (7) [9]. In an average sense, we verified an excellent agreement between analytical and numerical results. In $z = b_d$, an excellent agreement was also verified, except near the metallic pipe inner wall. This may be due to poor mesh refinement in that region leading to a relatively large staircase structure on the mesh boundaries. Fig. 3 presents the normalized axial electric field as a function of the normalized axial position for two radial positions, which are $\rho = 0$ (on axis) and $\rho = b_d$ (the edge of the charged disc). We verified an excellent agreement between analytical and numerical results. Additionally, we verified no divergence near the disc surface. It is due to the fact that when the observer becomes closer and closer to the disc surface, the electric fields becomes similar to that of a charged plane. Fig. 4 shows the normalized axial electric force between two concentric charged discs as a function of the normalized axial distance between then. The source disc is in $z_{d,s} = 0$, while the observer disc approximates by negative axial positions. We verify an excellent agreement between analytical and numerical results. Additionally, the analytic electric force does not diverge when the axial distance between the observer and the source discs tends to zero, as expected.

3.2. Ring particle results

In these plots, the source ring always has radius $b_r = a/2$ and stands on the axial position $z_r = 0$. The electric field plots show the

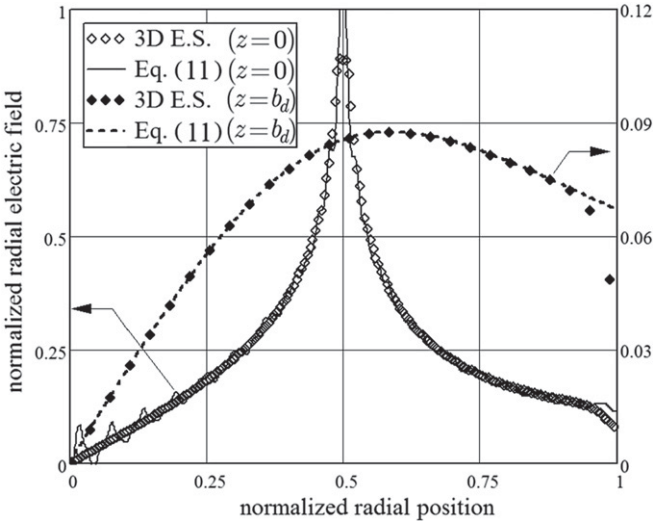

Fig. 2. The normalized radial electric field as function of the normalized radial position for two values of axial position, which are $z = 0$ and $z = b_d$.

main difference between our ring expression Eqs. (13) and (14) and those presented in [5]. Fig. 5 shows the normalized axial electric field generated by a ring source on axis ($\rho = 0$) as a function of the normalized axial position. A very similar result may be found in Fig. 3 of [10], which used an approach based on elliptic integrals. We observe that the reference expression [5] diverges when the observer becomes axially close to the source, what generates oscillatory noise on the axial force. On the other hand, Eq. (14) presented a smooth behavior in the same region. Fig. 6 shows the normalized radial electric field as a function of the normalized radial position in $z = b_r$. We observe that, in this case, our expression Eq. (13) diverges when the observer becomes radially close to the source coordinate, while reference expression presents smooth profile. Fig. 7 shows the normalized electric force between two electrically charged and concentric rings. In the numerical results, the source and the observer rings are identical. However, due to the divergence of the ring expressions when the source and the observer radial coordinates match, the observer ring has radius 2% smaller than the source one in the analytical results. Even so, we

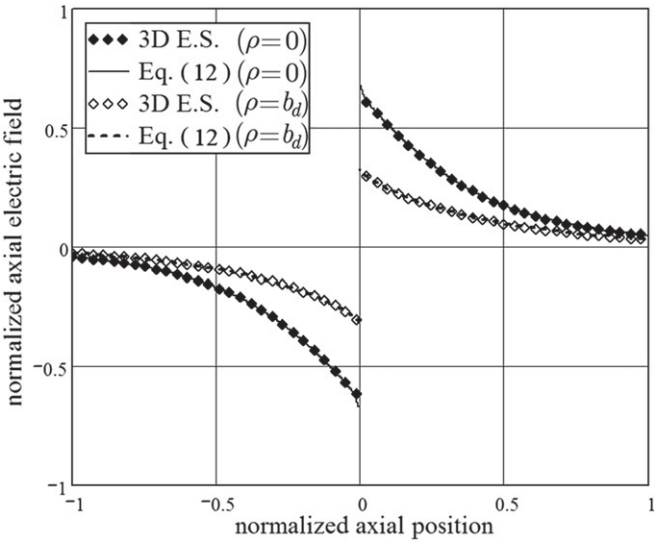

Fig. 3. The normalized axial electric field as function of the normalized axial position in two radial positions, which are $\rho = 0$ (on axis) and $\rho = b_d$ (the edge of the charged disc).

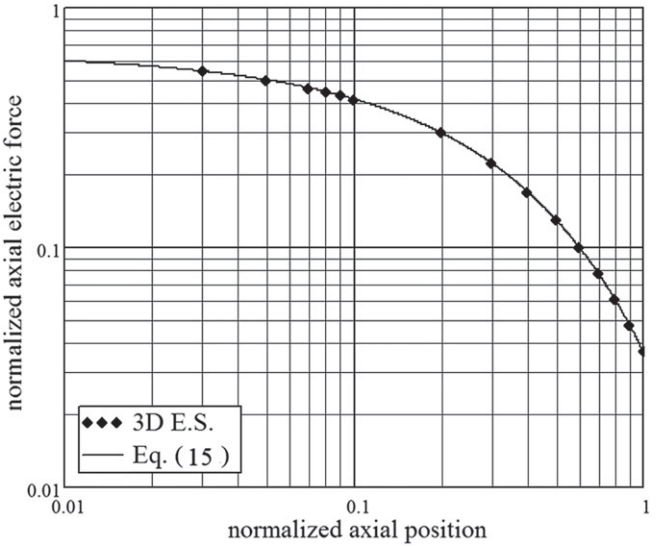

Fig. 4. The normalized electric force between two concentric charged discs as function of the normalized axial distance between them.

verified an excellent agreement between numerical and analytical results. The discrepancy appears when the normalized axial distance between rings tends to zero. For identical rings, the force diverges, while for rings with different radii the force vanishes.

3.3. Force between ring and disc

Fig. 8 shows the normalized axial electric force on an electrically charged ring with radius $b_r = a/2$ due to an electrically charged disc with radius $b_d = a/4$ at $z_d = 0$. Since the electric charges of both particles are positive (or negative), the force between then is always repulsive. As the ring approximates the disc, the force on it grows up until a maximum and then diminishes until vanishes at the same axial coordinate. When the ring passes over the disc, the repulsive force turns to grow up until a maximum position and then decays exponentially.

With respect to the time required to compute the forces, we can point out a dramatically difference between numerical and analytical calculations and a few time difference between integral

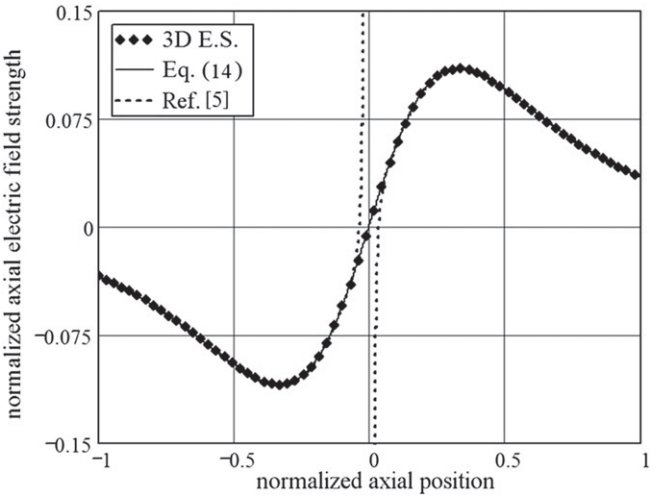

Fig. 5. The normalized axial electric field on axis ($\rho = 0$) as function of the normalized axial position for an electrically charged ring with radius $b_r = a/2$ at axial position $z = 0$.

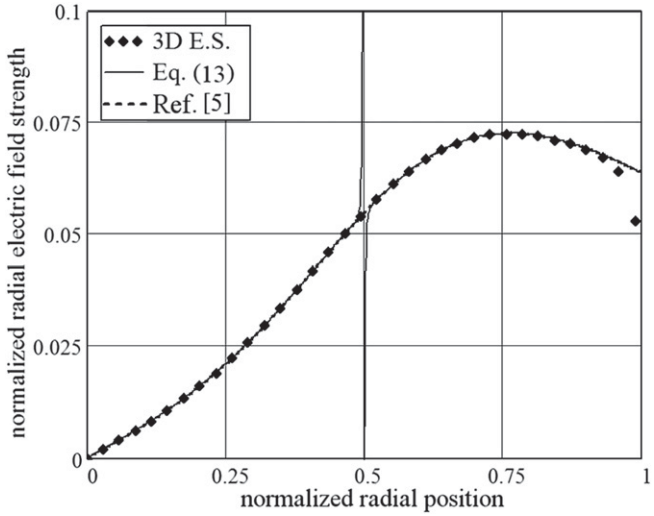

Fig. 6. The normalized radial electric field as function of the normalized radial position and $z = b_r$ for an electrically charged ring with radius $b_r = a/2$ at axial position $z = 0$.

and summation approaches. While integral and summation expressions take just some seconds to compute a whole plot with hundreds of points, a 3D electrostatic solver based on finite element methods [3] spent about 16 h to compute the results in Figs. 4 and 7 in a contemporary desktop computer. In the integral approach, the oscillatory noise problem may be mitigated by increasing the upper limit of the integral. Indeed, in this case, a higher upper limit means more computation time. Thus, a good trade off relation must be found.

3.4. The surface charge density and cosine Fourier transforms

The surface charge density induced $\sigma(z)$ can be evaluated from Eq. (11) or (13) by the definition $\sigma(z) = \varepsilon_0 \hat{\mathbf{n}} \cdot \mathbf{E}(a,z)$, where $\hat{\mathbf{n}}$ is the normal unity vector. So, using Eq. (11), one gets for the surface charge density induced by the disc,

$$\sigma_d(z) = \varepsilon_0 \mathbf{n} \cdot \mathbf{E}_d(a,z) = -\frac{q_d}{\pi a b_d} \sum_{n=1}^{\infty} \frac{J_1(x_{0,n} b_d/a)}{x_{0,n} J_1(x_{0,n})} e^{-\frac{x_{0,n}}{a}|z-z_d|}. \quad (20)$$

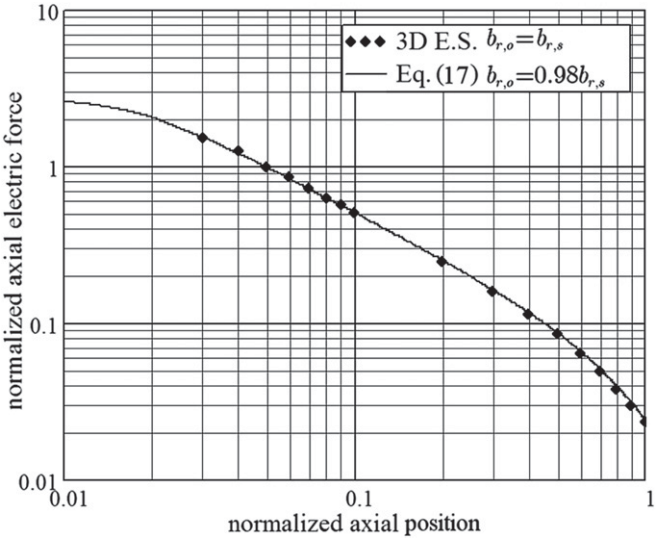

Fig. 7. The normalized axial electric force between two concentric electrically charged rings. The observer ring has radius $b_{r,o} = 0.98 b_{r,s}$, where $b_{r,s}$ is the source ring radius.

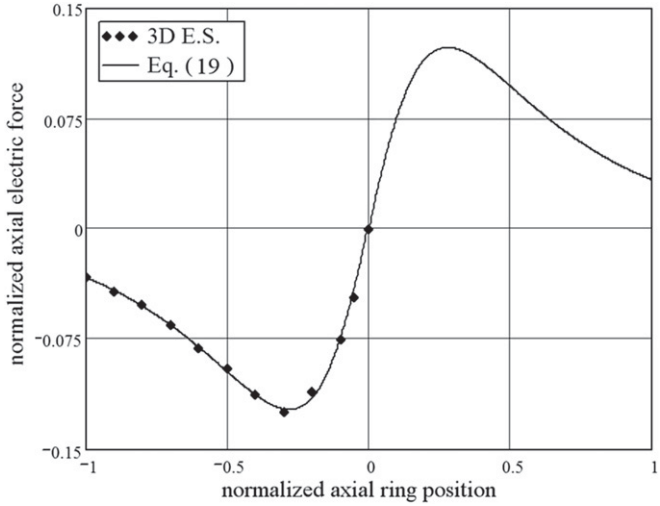

Fig. 8. The normalized axial electric force on an electrically charged ring with radius $b_r = a/2$ due to an electrically charged disc with radius $b_d = a/4$ standing at $z_d = 0$.

and using Eq. (13), one obtains for the surface charge density induced by the ring,

$$\sigma_r(z) = \varepsilon_0 \mathbf{n} \cdot \mathbf{E}_r(a,z) = -\frac{q_r}{2\pi^2 a} \int_0^{\infty} \frac{I_0(kb_r)}{I_0(ka)} \cos[k(z-z_r)]dk. \quad (21)$$

As shown in Fig. 9, both surface charge densities are even functions of $(z-z_d)$ and $(z-z_r)$, respectively, with their maximum values at z_d and z_r. Similar results can be obtained if the Green's functions Eqs. (7) and (8) are used to evaluate $\sigma(z)$ instead of Eqs. (8) and (7), respectively. Doing it, one gets the results for the disc and ring surface charge density induced,

$$\sigma_d(z) = -\frac{q_d}{\pi^2 a} \int_0^{\infty} \frac{1}{k} \frac{I_1(kb_d)}{I_0(ka)} \cos[k(z-z_d)]dk, \quad (22)$$

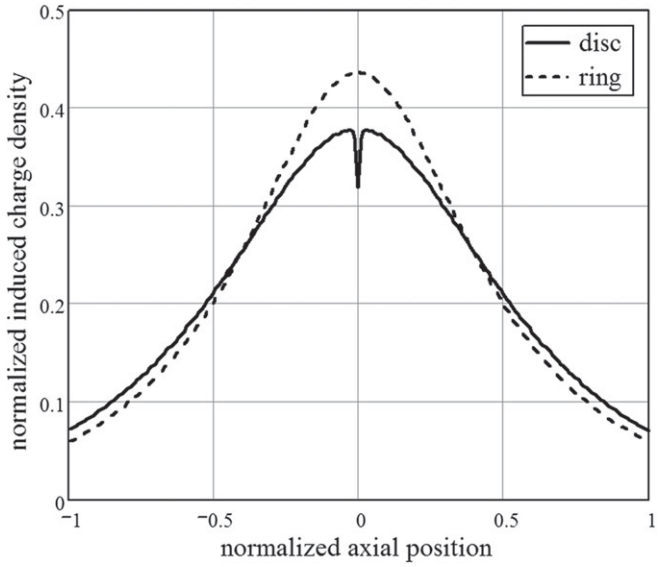

Fig. 9. The normalized induced charge densities on the inner pipe walls as a function of the normalized axial position. Solid line is for the disc source and the dashed line is for the ring source.

and

$$\sigma_r(z) = -\frac{q_d}{2\pi a^2}\sum_{n=1}^{\infty}\frac{J_0(x_{0,n}b_r/a)}{J_1(x_{0,n})}e^{-\frac{x_{0,n}}{a}|z-z_r|}. \tag{23}$$

By comparing Eqs. (20)–(22) and Eqs. (21)–(23), we can write the following results for cosine Fourier transforms, that we believe to be of some relevance. Indeed, at least to the author's knowledge, they were not previously published in Fourier transforms classic handbooks [11–13],

$$\int_0^{\infty}\frac{1}{k}\frac{I_1(kb_d)}{I_0(ka)}\cos[k(z-z_d)]dk = \frac{\pi}{b_d}\sum_{n=1}^{\infty}\frac{J_1(x_{0,n}b_d/a)}{x_{0,n}J_1(x_{0,n})}e^{-\frac{x_{0,n}}{a}|z-z_d|},\ b_d<a \tag{24}$$

$$\int_0^{\infty}\frac{I_0(kb_r)}{I_0(ka)}\cos[k(z-z_r)]dk = \frac{1}{a}\sum_{n=1}^{\infty}\frac{J_0(x_{0,n}b_r/a)}{J_1(x_{0,n})}e^{-\frac{x_{0,n}}{a}|z-z_r|},\ b_r<a \tag{25}$$

4. Conclusion

In this paper, we presented alternative expressions for the electric potential, the field, and the force between disc and ring charge distributions inside metallic pipe. These expressions are suitable for 2D or 2.5D space charge computation in pencil and hollow e-beams, commonly used in MVEDs. Force expressions developed here presented excellent agreements with numerical results and with other expressions, previously published in all cases, except when numerical noise due to field divergence takes place. Present ring force expressions were developed in order to avoid oscillatory noise when the field diverges by axial proximity between source and observer. The time computation presented little difference between summation and integral approaches, but presented dramatic difference between numerical and analytical approaches.

Acknowledgment

The authors wish to express their most sincere thanks to Editor M. N. Horenstein and Referees who read the manuscript carefully and gave valuable comments and help.

This work was supported in part by FAPESP (The State of São Paulo Research Agency) under project 2008/05286-1 and FINEP (Research and Projects Financing) under contract 01.09.0049.02

Appendix

In order to obtain Eq. (8), we expand the Green's function in terms of axial and azimuthal eigenfunctions that are solutions of the Laplace's problem in cylindrical coordinates. Therefore, we can write

$$G_2(\mathbf{r},\mathbf{r}') = \frac{1}{2\pi}\sum_{m=-\infty}^{\infty}\int_0^{\infty}\mathbf{G}_m(\rho,k,\mathbf{r}')e^{jm\varphi}[\cos(kz)+\sin(kz)]dk. \tag{A.1}$$

Substituting (A.1) in Eq. (5) and using orthogonality properties for the eigenfunctions assumed, we find

$$\frac{1}{\rho}\frac{d}{d\rho}\left(\rho\frac{d\mathbf{G}_m}{d\rho}\right)-\left(k^2+\frac{m^2}{\rho^2}\right)\mathbf{G}_m = -\frac{\delta(\rho-\rho')}{\rho}\pi e^{-jm\varphi'}[\cos(kz') + \sin(kz')], \tag{A.2}$$

which is an one-dimensional equation for Green's function problem. To simplify (A.2) we can define a new expansion coefficient for (A.1) and solution for (A.2) as

$$\mathbf{g}_m = \mathbf{G}_m/\pi e^{-jm\varphi'}[\cos(kz')+\sin(kz')]. \tag{A.3}$$

Then, if we observe the points where $\rho=\rho'$, (A.2) becomes the modified Bessel's equation for, say, ψ_m. The well known solution in this case is

$$\psi_m(\rho,k,\rho') = A(\rho')I_m(k\rho)+B(\rho')K_m(k\rho), \tag{A.4}$$

where $I_m(x)$ and $K_m(x)$ are the modified Bessel's functions of the first and second kind, respectively. In order to make the Green's function finite for $0\le\rho<\rho'$, we set $B(\rho')=0$.

On the other hand, to satisfy Eq. (6), for $\rho'<\rho\le a$, $B(\rho')=-A(\rho')I_m(ka)/K_m(k\rho)$. Thus we can write $\psi_m(\rho,k,\rho')$ for the two radial regions inside the metallic pipe, i.e.,

$$\psi_m(\rho)=\begin{cases}\psi_{1m}(\rho) = AI_m(k\rho) & 0\le\rho\le\rho'\\ \psi_{2m}(\rho) = B[I_m(k\rho)K_m(kb)-I_m(kb)K_m(k\rho)] & \rho'\le\rho\le a\end{cases}. \tag{A.5}$$

According to the Sturm-Liouville theory [14,15], the coefficient $\mathbf{g}_m(\rho,k,\rho')$ is given by

$$\mathbf{g}_m(\rho,k,\rho') = \begin{cases}-\dfrac{\psi_{1m}(\rho)\psi_{2m}(\rho')}{p(\rho')W(\rho')}, & 0\le\rho\le\rho'\\ -\dfrac{\psi_{1m}(\rho')\psi_{2m}(\rho)}{p(\rho')W(\rho')}, & \rho'\le\rho\le a\end{cases}, \tag{A.6}$$

where $W(\rho')$ is the wronskian determinant. Due to the Green's functions properties, one can verify that $p(\rho')W(\rho') = ABI_m(ka)$. Thus, developing (A.6), we found

$$\mathbf{g}_m(\rho,k,\rho') = \begin{cases}I_m(k\rho)\left[K_m(k\rho')-\dfrac{K_m(ka)}{I_m(ka)}I_m(k\rho')\right], & 0\le\rho<\rho'\\ I_m(k\rho')\left[K_m(k\rho)-\dfrac{K_m(ka)}{I_m(ka)}I_m(k\rho)\right], & \rho'<\rho\le a\end{cases} \tag{A.7}$$

Using (A.7), (A.3), (A.1), and a few more algebra, we find Eq. (8).

On the other hand, in order to obtain Eq. (7), we expand the Green's function in terms of radial and azimuthal eigenfunctions, solutions of the Laplace's problem in cylindrical coordinates. Thus

$$G_1(\mathbf{r},\mathbf{r}') = \sum_{m=-\infty}^{\infty}\sum_{n=1}^{\infty}\mathbf{G}_m(z,\mathbf{r}')J_m(x_{m,n}\rho/a)e^{jm\varphi}, \tag{A.8}$$

where $x_{m,n}$ is the n-th zero of $J_m()$, that is the ordinary Bessel's function of order m. Substituting (A.8) in Eq. (5) and carrying out the algebra, we find

$$\nabla^2 G_1(\mathbf{r},\mathbf{r}') = \sum_{m=-\infty}^{\infty}\sum_{n=1}^{\infty}\left[\frac{d^2\mathbf{G}_m}{dz^2}-\frac{x_{m,n}}{a^2}\mathbf{G}_m\right]J_m(x_{m,n}\rho/a)e^{jm\varphi}. \tag{A.9}$$

With the help of the orthogonality properties for the Bessel's function and for the exponential function, we can handle (A.9) to obtain

$$\frac{d^2\mathbf{G}_m}{dz^2}-\left(\frac{x_{m,n}}{a}\right)^2\mathbf{G}_m = -\delta(z-z')\frac{J_m(x_{m,n}\rho'/a)}{\pi a^2 J_{m+1}^2(x_{m,n})}e^{-jm\varphi'}. \tag{A.10}$$

Then, if we look at that points where $z\ne z'$, (A.10) becomes a simple eigenfunction problem. The well known solution in this case is

$$\mathbf{G}_m(z,z') = \begin{cases} \mathbf{G}_{1m}(z,z') = A_m(z')e^{-\frac{x_{m,n}}{a}z}, & z \le z' \\ \mathbf{G}_{2m}(z,z') = B_m(z')e^{\frac{x_{m,n}}{a}z}, & z \ge z' \end{cases}. \tag{A.11}$$

In order to determine the constants $A_m(z')$ and $B_m(z')$, we analyze the conditions for the continuity of the Green's function at $z = z'$ and the value of the discontinuity of its first derivative at the same position. After a lengthy, but well known algebra, we obtain

$$\mathbf{G}_m(z,\mathbf{r}') = \begin{cases} \dfrac{1}{2\pi a}\dfrac{J_m(x_{m,n}\rho'/a)}{x_{m,n}J_{m+1}^2(x_{m,n})}e^{-jm\varphi'}e^{\frac{x_{m,n}}{a}(z-z')} & z \le z' \\ \dfrac{1}{2\pi a}\dfrac{J_m(x_{m,n}\rho'/a)}{x_{m,n}J_{m+1}^2(x_{m,n})}e^{-jm\varphi'}e^{-\frac{x_{m,n}}{a}(z-z')} & z \ge z' \end{cases}. \tag{A.12}$$

Substituting (A.12) in (A.8), we obtain the Green's function presented in Eq. (7).

References

[1] R.J. Baker, J.H. Booske, N.C. Luhmann Jr., G.S. Nusinovich, Modern Microwave and Millimeter-wave Power Electronics, IEEE Press, Piscataway, NJ, 2005.

[2] B. Goplen, L. Ludeking, D. Smithe, G. Warren, User-configurable MAGIC for electromagnetic PIC calculations, Computer Physics Communications 87 (1995) 54–86.

[3] CST STUDIO SUITE™, B User's Manual see also: (2006) www.cst.com.

[4] J.G. Wöhlbier, J. Booske, I. Dobson, On the physics of harmonic injection in a traveling wave tube, IEEE Transactions on Plasma Science 32 (3) (June 2004) 1073–1085.

[5] B.E. Carlsten, W.B. Haynes, W.T. Roybal, P.J. Tallerico, Green's function simulation of space–charge effects in electron beams, IEEE Transactions on Plasma Science 34 (5) (Oct. 2006) 2404–2413.

[6] S. Gómez-Moñivas, L.S. Froufe-Pérez, A.J. Caamaño, J.J. Sáenz, Electrostatic forces between sharp tips and metallic and dielectric samples, Applied Physics Letters 79 (24) (Dec 2001) 4048–4050.

[7] G.M. Sacha, C. Gómez-Navarro, J.J. Sáenz, J. Gómez-Herrero, Quantitative theory for the imaging of conducting objects in electrostatic force microscopy, Applied Physics Letters 89 (2006) 173122.

[8] J.A. Hernandes, A.K.T. Assis, Electric potential due to an infinite conducting cylinder with internal or external point charge, Journal of Electrostatic 63 (2005) 1115–1131.

[9] A. Peskoff, Green's function for Laplace's equation in an infinite cylindrical cell, Journal of Mathematical Physics 15 (1974) 2112–2120.

[10] P. Zhu, Field distribution of a uniformly charged circular arc, Journal of Electrostatic 63 (2005) 1035–1047.

[11] I.S. Gradshteyn, I.M. Ryzhik, Table of Integrals, Series, and Products, fourth ed. Academic, NY, 1965, p. 361.

[12] A. Erdély (Ed.), Tables of Integrals Transforms, vol. I, McGraw-Hill, 1954.

[13] A.P. Prudnikov, Y.A. Brychkov, O.I. Marichev, Integrals and Series, , In: Special Functions, vol. 2, Gordon and Breach Science Publishers, 1988.

[14] R.E. Collin, Field Theory of Guided Waves, second ed. IEEE Press, NY, 1991, pp. 55–78.

[15] J.D. Jackson, Classical Electrodynamics, second ed. John Wiley & Sons, NY, 1975, pp. 116–118.